Tech Science Press

Experimental and Numerical Investigation on the External Aerodynamic Noise of High-Speed Train

Shijie Jiang*, Song Yang, Bohong Zhang and Bangchun Wen

School of Mechanical Engineering & Automation, Northeastern University, Shenyang, 110819, China.

*Corresponding Author: Shijie Jiang. Email: jiangsj@me.neu.edu.cn.

Abstract: Aerodynamic noise is the dominant noise source of the high-speed train. It not only seriously affects the passenger comfort and people's normal life along the railway line, but also may cause fatigue damage to the surrounding equipment and buildings. This manuscript carried out the simulation and experimental study on the external aerodynamic noise of high-speed train, in order to increase the understanding of the noise and hence to be better able to control it. The on-line tests were performed to verify that it is reasonable to simplify the high-speed train model. The turbulent air flow model was then developed, and the external steady flow field was computed by Realizable k-ε turbulence model. Based on the steady flow field, aerodynamic noise sources on the train surface and the external transient flow field were calculated by broadband acoustics source model and large eddy simulation (LES) respectively. The pressures on the train surface were obtained from the results of the transient model. Considering the transient flow field, the far-field aerodynamic noise generated by the high-speed train was finally obtained based on Lighthill-Curle theory. Through the comparison between simulations and on-line tests, it is shown that the numerical model gives reliable aerodynamic noise predictions. This research is significant to the study and control of the aerodynamic noise of high-speed train.

Keywords: High-speed train; aerodynamic noise; Lighthill-Curle theory; simulated analysis; on-line test

1 Introduction

With the development of technology, the train speed has been greatly increased, which makes some problems that can be ignored at low speed become rather serious, and thus constrained the development of high-speed train technology severely. One of the problems is noise, mainly including wheel-rail noise and aerodynamic noise [1,2]. The wheel-rail noise has been controlled effectively with the deep understanding of its generation mechanism, while the high speed of train makes the aerodynamic noise increasingly severe [3,4]. When a train is cruising at high speeds, normally above 250 km/h, aerodynamic noise becomes the dominant source [5]. It not only seriously affects the passenger comfort and people's normal life along the railway line, but also may cause fatigue damage to the surrounding equipment and buildings, which greatly restricts the sustainable development of high-speed railways. Therefore, there are important theoretical value and practical significance in studying the simulation and control method on aerodynamic noise of high-speed train.

At present, mainly two means are performed to study the flow and noise around a high-speed train: numerical and experimental research. The existing experimental research is mostly carried out based on wind tunnel test, which investigates the characteristics of air flow and its interaction with the train scaling model in a wind tunnel. According to the similarity principle, the aerodynamic characteristics of a real train would be understood. However, the wind tunnel test is a kind of simulation test, and there are obvious limitations, such as boundary interference, holder interference, low Reynolds number, high cost,

etc. [6]. About the numerical research [7], simulation technology of fluid dynamics has been widely utilized to study the aerodynamic noise of high-speed train. However, the relevant on-line tests are few; the past numerical research generally lacks validation. In this paper, the Lighthill-Curle theory [8-10] is used in the simulation calculation. The steady flow field was simulated first, followed by the calculation of surface noise source and the transient flow field, then the far field aerodynamic noise simulation results were obtained. In addition, series of on-line tests were performed with a self-made test platform along a real high-speed railway line. Through the comparison between predictions and measurements, the simulation model was validated and the characteristics of the aerodynamic noise were obtained. This research provides the basis and technical support for simulation and control on the aerodynamic noise generated by a whole train.

In this paper, the on-line test method of aerodynamic noise of high speed train is introduced, and the full size three-dimensional simplified train model is set up according to the result in Section 2. Simulation methodology is introduced and the predictions of aerodynamic noise generated by the high-speed train were obtained in Section 3, followed by corresponding results and discussions in Section 4. Section 5 summarizes the conclusions.

2 On-Line Test

At present, the high-speed railways are generally built on viaducts, in order to avoid foundation settlement, ensure safety, reduce cost and so on. The railways height could be up to 11 meters, and they are mostly far away from the urban area with complex terrains. These cause it difficult to directly measure the aerodynamic noise of high-speed train. In this paper, series of on-line tests have been performed along a high-speed railway line using a self-designed aerodynamic noise collection platform, mainly including microphone (BSWA-MP201), NI USB-4431 data acquisition card, tachymeter (Bushnell 101921), laptop and so on, as shown in Fig. 1. The laser rangefinder was mainly used to determine the position of microphones, and the tachymeter was used to test the train speed. When the train (CRH380B) was passing by, the real-time signal (like noise and speed) was recorded and the on-line test was completed. Compared with wind tunnel test, the on-line test is more accurate and cost-saving.

(a) Tachymeter (b) Laser rangefinder (c) Noise collection system

Figure 1: On-line test equipment

Two microphones were positioned to receive aerodynamic noise at different heights. According to ISO 3095:2005, one was 7.5 m from the railway central line and 3.5 m above the rail head; and the other was the same distance from the railway central line but 1.5 m above the rail head, as shown in Fig. 2.

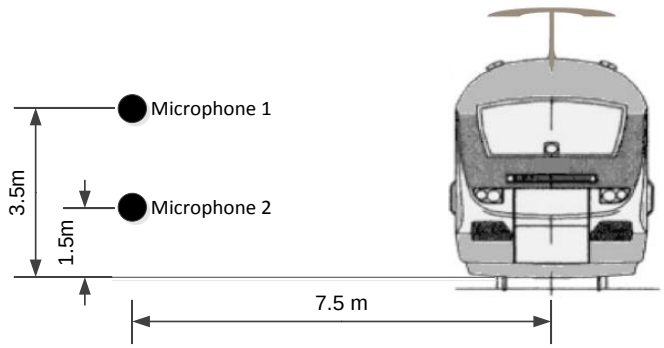

Figure 2: Monitoring points for measuring aerodynamic noise

To measure the aerodynamic noise of high-speed train, the influence of environmental background noise has to be taken into consideration. Therefore, multiple groups of environmental noise signals were recorded when there was no train passing by. To ensure the accuracy and reliability, totally 5 groups of background noise and 20 groups of real-time aerodynamic noise of high-speed train were measured. Fig. 3 shows an example of the comparison between aerodynamic noise and background noise in time domain.

From Fig. 3, it can be seen that the aerodynamic noise is obviously higher than background noise. According to the principle of noise superposition ($L = 10\lg\left(10^{L_1/10}+10^{L_2/10}+\cdots+10^{L_N/10}\right)$), if the difference of two noise sources in sound pressure level is more than 10 dB, the source with larger SPL can be the result of superposition (with the deviation less than 0.4 dB). In addition, the peak values of aerodynamic noise, much higher than other parts, are separately generated by the head car and tail car (as shown in Fig. 3). Since the car body surface is smooth, and the curvature change is small, it contributes less to the overall noise. Therefore, shortening the car body will not influence the distribution of the sound power level generated by the train surface.

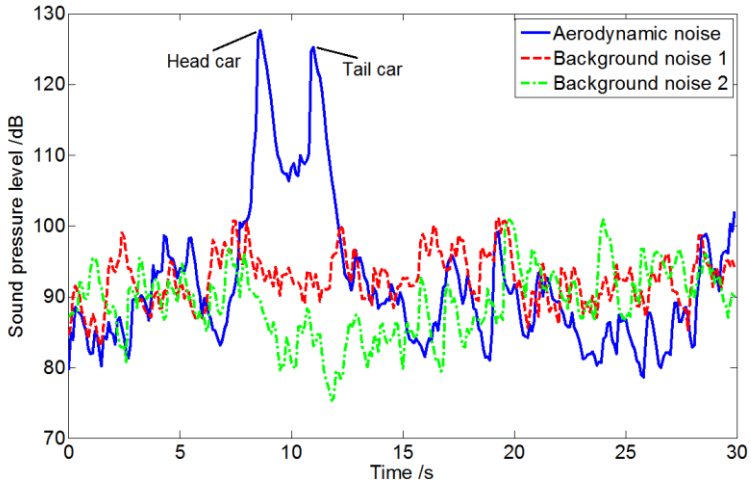

Figure 3: Aerodynamic noise and background noise

3 Simulation Methodology

The simulation of the aerodynamic noise of high-speed train mainly includes: 1) Calculating steady flow field by Realizable k-ε turbulence model, 2) simulating train surface noise sources by broadband noise source model, 3) obtaining the static pressures of the train surface based on the transient flow field calculated by the Large Eddy Simulation (LES) method and 4) figuring out the far field aerodynamic noise of high-speed train power car by Lighthill-Curle theory with the transient flow field results.

3.1 3D Modelling

The experimental analysis shows that the car body length has little influence on the overall aerodynamic noise. Therefore, a full-size three-dimensional simplified model was built up for the high-speed train (CRH380B type). It was modeled by using the head car and tail car instead of the whole train, which will not change the rule and characteristic of the train body's acoustic power distribution. This can also simplify the calculation and improve the simulation efficiency. The model's length, width and height were 51400 mm, 3400 mm and 3700 mm, respectively. To further increase the simulating rate, windows, doors and bogies were simplified, as shown in Fig. 4.

Figure 4: 3D model of the whole train

To make sure that the flow field around the vehicle was not influenced, the external flow field boundary had to be large enough. Therefore, it was defined as a rectangle, and the distances were 20 m between its entrance boundary and the car front-end, 40 m between the exit boundary and the rear-end, and 20 m between the lateral boundary and the central line of the vehicle. Since the train is symmetric, only half of the model was analyzed to further improve the simulation efficiency. The hybrid grid method was adopted to mesh the model, with the train meshed with triangle and quadrilateral elements and the external flow field meshed with tetrahedron (primary) and hexahedron (auxiliary) elements. Due to the complexity of the gas flowing on body surface, three boundary layers of triangular prism were generated on the vehicle surface. The thickness was 1.25, 1.5 and 1.8 mm thick, respectively. The total number of mesh is about six million. Details are shown in Fig. 5.

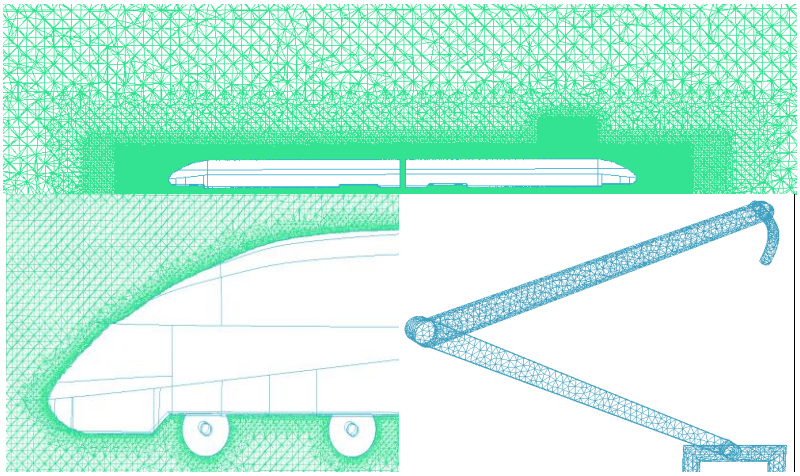

Figure 5: Mesh structure of the vehicle and flow field

3.2 Steady State Simulation

At present, the train speed is far lower than the sound speed (340 m/s) and the Mach number is far less than 1, therefore, the surrounding air can be regarded as incompressible viscous fluid, the basic control equations are as follows:

$$\frac{\partial u_i}{\partial x_i} = 0 \tag{1}$$

$$\partial u_i + u_j \frac{u_i}{x_j} = -\frac{1}{\rho}\frac{\partial p}{\partial x_i} + \frac{\mu}{\rho}\frac{\partial^2 u_i}{\partial x_j x_j} \tag{2}$$

where u_i is the velocity component of the fluid (air) surrounding the train in the x direction, $i = 1, 2, 3$, $j = 1, 2, 3$, and $i \neq j$; ρ and p are the density and pressure of the surrounding flow field; μ is the air dynamic viscosity coefficient.

The turbulence flow could be described by the Navier-Stokes (N-S) equation, and the steady state calculation was carried out based on the Realizable $\mathbf{k}$-$\boldsymbol{\varepsilon}$ model [11]. This model is suitable for various types of flow (like spin uniform shear flow, channel flow and boundary layer flow, etc.), and the simulation results are reliable. The model is based on the transport equations of the two variables, i.e., the turbulence kinetic energy ($\mathbf{k}$) and the dissipation rate ($\boldsymbol{\varepsilon}$), respectively. The equations are defined as follows:

$$\frac{\partial(\rho k)}{\partial t} + \frac{\partial(\rho k u_i)}{\partial x_i} = \frac{\partial}{\partial x_i}\left[\left(\mu + \frac{\mu_t}{\sigma_k}\right)\frac{\partial k}{\partial x_i}\right] + G_k \tag{3}$$

$$\frac{\partial(\rho \varepsilon)}{\partial t} + \frac{\partial(\rho \varepsilon u_i)}{\partial x_i} = \frac{\partial}{\partial x_i}\left[\left(\mu + \frac{\mu_t}{\sigma_\varepsilon}\right)\frac{\partial k}{\partial x_i}\right] + G_\varepsilon \tag{4}$$

where $G_k = P_k - D_k$, P_k is the production term and $P_k = \tau_{ij}^t \frac{\partial u_i}{\partial x_j}$; D_k is the Dissipative term and $D_k = \rho\varepsilon$; $G_\varepsilon = P_\varepsilon - D_\varepsilon$, P_ε is the production term and $P_\varepsilon = C_1 \frac{\varepsilon}{k} \tau_{ij}^t \frac{\partial u_i}{\partial x_j}$; D_ε is the Dissipative term and $D_\varepsilon = C_2 \rho \frac{\varepsilon^2}{k}$; μ_t is the turbulence viscosity coefficient and $\mu_t = \rho C_\mu \frac{k^2}{\varepsilon}$. In these equations, σ_k, σ_ε, C_1, C_2, C_μ are empirical constant and they were 1.0, 1.3, 1.44, 1.92 and 0.09, respectively. The main parameters settings in the steady state flow field simulation are shown in Tab. 1.

Table 1: Steady state flow field simulation settings

Category	Contents	Setup
General	Solver Type	Pressure-Based
	Time	Steady
Models	k-epsilon	Realizable
Materials	Air	
Boundary Conditions	Inlet	Velocity inlet v = 83.3 m/s k = 0.2604 m^2/s^2 ε = 0.0273 m^2/s^3
	Outlet	Pressure outlet
	Ground	Wall
	Fluid domain surface	Symmetry
	Fluid domain	Interior
Run Calculation	Number of Iterations	2000

3.3 Aerodynamic Noise Source Calculation

Ignoring the differential of time delay (replaced by covariance equivalent synchronization), Proudman obtained the radiated acoustic power P_A of isotropic turbulence per unit volume deduced by

Acoustic analogy theory under the condition of low Mach number and high Reynolds number [12], the expression is:

$$P_A = \alpha\rho_0\left(\frac{u^3}{l}\right)\frac{u^5}{c_0^5} \tag{5}$$

where α is a model constant, ρ_0 is the average fluid density without disturbance, u is fluid speed, l is the turbulence length and c_0 is sound speed. In the form of k and ε, it can be expressed as $P_A = \alpha_\varepsilon\rho_0\varepsilon M_t^5$, and $M_t = \sqrt{2k}/c_0$.

Sarker and Hussaini [13] calculated the isotropic turbulence with the direct numerical simulation method, obtaining 0.1 for α_ε. Based on the steady state calculation of the turbulence model, the turbulence kinetic energy and dissipation rate of each node in the flow field were extracted, and the sound power of each node was obtained, with which the distribution of the sound power level on the vehicle surface was worked out.

3.4 Transient State Simulation

Transient state calculation was performed by the large eddy simulation (LES) model [2], whose core meaning is that filtering the vortices less than a certain scale in the transient flow field, then the rest of the large eddies could be obtained by N-S equations. They are expressed as:

$$\frac{\partial\rho}{\partial t} + u\frac{\partial\rho\overline{u_i}}{\partial x_i} = 0 \tag{6}$$

$$\frac{\partial}{\partial t}(\rho\overline{u_i}) + \frac{\partial}{\partial x_j}(\rho\overline{u_i u_j}) = \frac{\partial}{\partial x_j}\left(u\frac{\partial\overline{u_i}}{\partial x_j}\right) - \frac{\partial\bar{p}}{\partial x_j} - \frac{\partial\tau_{ij}}{\partial x_j} \tag{7}$$

where $\overline{(\ )}$ is the spatial filtering, $\overline{u_i}$ is the time-average speed, $\bar{p}$ is the time-average pressure, t is time, τ_{ij} is the sub grid-scale stress, $\tau_{ij} = \rho\overline{u_i u_j} - \rho\overline{u}_i\overline{u}_j$ ($\rho\overline{u_i u_j}$ is Reynolds stress), which embodies the effect of small-scale eddies on the equation of motion. The main parameter settings in the transient flow field simulation are shown in Tab. 2.

Table 2: Transient state simulation settings

Category	Contents	setup
General	Solver Type	Pressure-Based
	Time	Transient
Models	LES	
Materials	Air	
Boundary Conditions	Inlet	Velocity inlet v=83.3m/s
	Outlet	Pressure outlet
	Ground	Wall
	Fluid domain surface	Symmetry
	Fluid domain	Interior
Run Calculation	Number of Iterations	4000

3.5 Far-Field Aerodynamic Noise Simulation

The far-field aerodynamic noise of high-speed train was simulated by Acoustic analogy method deduced by Lighthill [9,10] based on Navier-Stokes (N-S) equation and continuity equation. The sound propagation can be expressed as

$$\frac{\partial^2 \rho'}{\partial t^2} - \nabla^2 p' = \frac{\partial^2 T_{ij}}{\partial x_i \partial x_j} \tag{8}$$

where T_{ij} is Lighthill turbulence stress tensor, $T_{ij} = \rho v_i v_j + \delta_{ij}[(p - p_0) - c_0^2(\rho - \rho_0)] - e_{ij}$, v_i, v_j are speed vectors, δ_{ij} is the unit tensor, ρ_0 and p_0 are the average fluid density and pressure without disturbance, e_{ij} is the fluid viscous stress tensor, ρ' and p' are the fluctuating values of fluid density and pressure, and $\rho' = \rho - \rho_0$, $p' = p - p_0$.

When there is a solid wall boundary in unsteady flow field, the solution to Lighthill equation deduced by Curle [14] yields:

$$\rho'(x,t) = \frac{1}{4\pi c_0^2}\left[\frac{\partial^2}{\partial x_i' x_j'}\int_v \frac{T_{ij}(y, t - R/c_0)}{R} dy - \frac{\partial}{\partial x_i'}\int_S \frac{n_j P_{ij}(y, t - R/c_0)}{R} dy\right] \tag{9}$$

where n_j is the cosine of the outward direction (pointing to the fluid) perpendicular to the solid wall, P_{ij} is the fluctuating pressure on the vehicle surface, *y* is the sound source point vector, *x* is the receiver point vector, $R = x - y$.

There are two types of noise source [11] included in Eq. (9): the first term of the right hand side is dipole noise source (derived from the Lighthill stress of the flow field around the vehicle) and the other one is quadrupole source (from the vehicle's surface pressure and viscous shear stress). Since the dipole source noise and quadrupole source noise are respectively proportional to the third power and fifth power of Mach number, the ratio of the quadrupole source noise to the dipole source noise is proportional to the square of Mach number. As the Mach number of the vehicle is about 0.245 under the present running speed (around 300 km/h), the quadrupole source noise is relatively smaller, and it can be ignored. Therefore, the formula for calculating the aerodynamic noise of high-speed train can be expressed as

$$\rho'(x,t) = -\frac{1}{4\pi c_0^2}\frac{\partial}{\partial x_i'}\int_S \frac{n_j P_{ij}(y, t - R/c_0)}{R} dy \tag{10}$$

$$P(x,t) - P_0 = c_0^2 \rho'(x,t) \tag{11}$$

where *P* is sound pressure, and P_0 is the reference sound pressure, $P_0 = 2 \times 10^{-5} Pa$.

According to the results of the transient state simulation, the fluctuating pressure of each node on the vehicle surface can be extracted, based on which the far-field aerodynamic noise pressures of high-speed train could be worked out with Eq. (11).

To compare the simulated and measured aerodynamic noise, two monitoring points were set in the flow field to record the noise generated by the train passing by. The positions were the same as those of the microphones mentioned in the experiment, as shown in Fig. 2. They were 1.5 m and 3.5 m above the rail head, respectively, and 7.5 m away from the railway central line.

4 Results and Discussion

As shown in Fig. 6, a positive pressure area occurs at the train head with a large gradient due to the area compressed by air, and the positive pressure is up to 4220 Pa; The joint between the front window and the car body is non-streamlined, which results in relatively high positive pressure (up to 2240 Pa); Since the curvature of the transition from train head to body changes obviously, the flow speed of the fluid becomes higher and its direction is to the inclined top of the train. It causes vacuum around the car body, and the positive pressures decreases to negative pressures, with the negative pressure down to -1710 Pa, appearing on the top and side chamber surfaces of the transition from the train head to the body; While due to the extremely irregular shape of the bogie (at the bottom of the vehicle), fluid flow was severe and complicated, causing the highest positive pressure, which is 5210 pa.

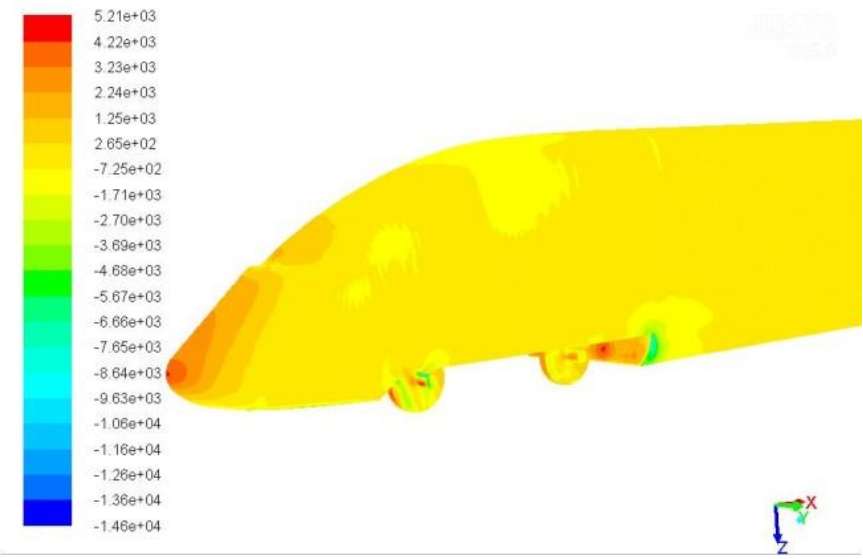

Figure 6: Static pressure chart of the train head

From Fig. 7, it can be seen that there are corresponding trends in source power levels that are attributed to the changed static pressures as shown in Fig. 6. Since the positive pressures at the areas of train head and front window are high, the corresponding aerodynamic noise is high; At the top and side chamber surfaces of the transition from the train head to the body, the negative pressure becomes maximum due to the interaction between vehicle surface and the external flow field, noise levels are relatively high; The surface of the vehicle body is smooth, with small curvature changes, the fluid flow is stable and noise levels are relatively low; while the sound power levels generated by the bogie are the highest, and it is because the bogie's shape is extremely irregular that results in severe and complicated turbulence flow.

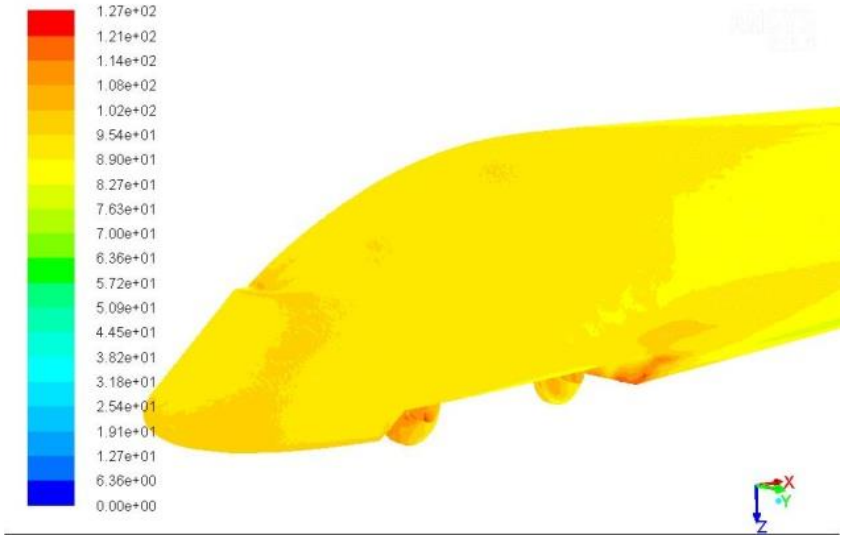

Figure 7: Noise source power level chart of the train head

The comparisons between simulations and measurements in A-weighted SPL of 1/3 octave band are shown in Figs. 8 and 9. Generally, it can be seen that the aerodynamic noise of high-speed train is a type

of broadband noise, i.e., there is no obvious frequency band, and the noise energy is continuously distributed in a wide frequency scope (0-5000 Hz).

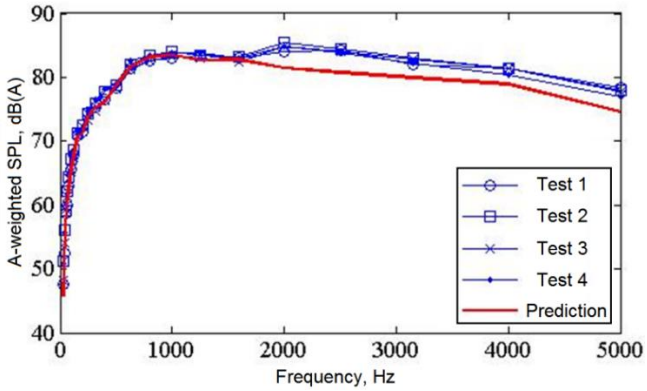

Figure 8: 1/3 octave band A-weighted SPL at Monitor 1

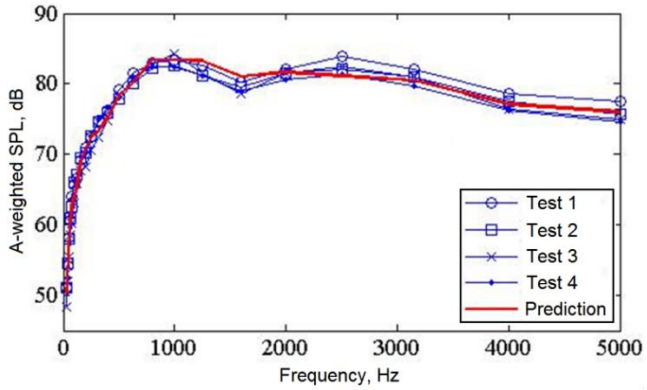

Figure 9: 1/3 octave band A-weighted SPL at Monitor 2

For Monitor 1 (shown in Fig. 8), the simulations agree well with the measurements in the frequency range from 0 to 1600 Hz. While above 1600 Hz, there are slight under-predictions with the difference less than 5%. About Monitor 2, it can be seen from Fig. 9 that the simulation results have a good agreement with the measurements in the whole frequency range. Therefore, the simulations and measurements are in good agreement, and the simulation model is reliable.

5 Conclusions

In this paper, experimental research on aerodynamic noise of high-speed trains was firstly carried out to confirm the rationality of the simplified train model. Simulations on the aerodynamic noise were then performed. Comparing the simulated and measured noise results, the detailed conclusions are as follows:

1) Shortening the train body length reasonably would not influence the distribution of the sound power level generated by the train surface.
2) Aerodynamic noise of high-speed train is linearly correlated with surface pressure. The greater the surface pressure is, the higher aerodynamic noise is generated.
3) The aerodynamic noise of high-speed train is a type of broadband noise, i.e., there is no obvious frequency band, and the noise energy is continuously distributed in a wide frequency scope (0-5000 Hz).

4) The simulated aerodynamic noise agrees well with the measurement, and the simulation model is reliable.

Acknowledgements: The work described has been supported by National Natural Science Foundation of China (51705068), the fundamental research funds for the central universities (N150303003) and research initiation funds for the PhD of Liaoning Province (201601005).

References

1. Sassa, T., Sato, T., Yatsui, S. (2001). Numerical analysis of aerodynamic noise radiation from a high-speed train surface. *Journal of Sound and Vibration, 247*, 407-416.
2. Liu, J. (2009). *The theoretical research and numerical simulation of aerodynamic noise of high-speed train (Ph.D. Thesis)*. Vehicle and Operation Engineering, Southwest Jiaotong University.
3. Zhu, J., Hu, Z., Thompson, D. J. (2013). Analysis of aerodynamic and aeroacoustic behaviour of a simplified high-speed train bogie. *Noise and Vibration Mitigation for Rail Transportation Systems: Proceedings of the 11th International Workshop on Railway Noise*, 489-496.
4. Yang, W., Kim, D., Park, J., Koh, H. (2013). Analysis on the aeroacoustic sound radiation from high-speed train using a simplified numerical model. *20th International Congress on Sound and Vibration*, 397-399.
5. Raghu, S. R., Kim, H. D., Setoguchi, T. (2002). Aerodynamics of high-speed railway train. *Progress in Aerospace Sciences, 38*, 469-514.
6. Ricco, P., Baronb, A., Molteni, P. (2007). Nature of pressure waves induced by a high-speed train travelling through a tunnel. *Journal of Wind Engineering and Industrial Aerodynamics, 95*, 781-808.
7. Lyu, B., Dowling, A. P., Naqavi, I. (2017). Prediction of installed jet noise. *Journal of Fluid Mechanics, 811*, 234-268.
8. Williams, J. E. F., Hawkings, D. L. (1969). Sound Generation by Turbulence and Surfaces in Arbitrary Motion. *Philosophical Transactions of the Royal Society of London, 264*, 321-342.
9. Lighthill, M. J. (1954). On sound generated aerodynamically: Part II: turbulence as a source of sound. *Proceedings of the Royal Society of London*, 1-32.
10. Lighthill, M. J. (1952). On Sound generated aerodynamically: Part I: general theory. *Proceedings of the Royal Society of London, 211*, 564-587.
11. Zheng, Z. (2012). *A study on the numerical simulation of high-speed vehicle's external aerodynamic acoustics field (Ph.D. Thesis)*. Southwest Jiaotong University.
12. Proudman, I., Pearson, J. (1957). Expansions at small Reynolds numbers for the flow past a sphere and a circular cylinder. *Journal of Fluid Mechanics, 2*, 237-262.
13. Sarkar, S., Erlebacher, G., Hussaini, M. Y., Kreiss, H. O. (1991). The analysis and modelling of dilatational terms in compressible turbulence. *Journal of Fluid Mechanics, 227*, 473-493.
14. Curle, N. (1955). The Influence of Solid Boundaries upon Aerodynamic Sound. *Proceedings of the Royal Society of London, 231*, 506-514.